Available online at www.sciencedirect.com

ScienceDirect

Ceramics International 40 (2014) 1251–1255

CERAMICS INTERNATIONAL

www.elsevier.com/locate/ceramint

Short communication

A nanocomposite of needle-like MnO_2 nanowires arrays sandwiched between graphene nanosheets for supercapacitors

Hongfang Song, Xinlu Li*, Yonglai Zhang, Hao Wang, Hongyi Li, Jiamu Huang

School of Materials Science and Engineering, Chongqing University, Chongqing 400030, PR China

Received 20 March 2013; received in revised form 13 June 2013; accepted 13 June 2013
Available online 19 June 2013

Abstract

A nanocomposite of needle-like MnO_2 nanowires arrays-graphene (NMNAG) is synthesized by in-situ growth of MnO_2 nanowires on the surface of graphene nanosheets (GNS), resulting in a sandwich nanoarchitecture hybrid. The preparation is a simple redox reaction between potassium permanganate ($KMnO_4$) and GNS, which is facile to produce in large scale at low cost. The nanocomposite exhibits high-capacitance performance (276 F g^{-1} at 0.5 A g^{-1}), excellent rate capability (62.7% capacity retention at 60 A g^{-1}), stable cycleability (no degradation after 1200 cycles) and a maximum power density of 21.6 kW kg^{-1}.
© 2013 Elsevier Ltd and Techna Group S.r.l. All rights reserved.

Keywords: Graphene; Manganese dioxide; Supercapacitor

1. Introduction

Supercapacitors (SCs), have been studied extensively in the past few decades as energy storage devices due to their higher power density than batteries, and higher energy density than conventional dielectric capacitors [1]. Currently, graphene nanosheets (GNS), as two-dimensional layers of sp^2-bonded carbon [2], have been regarded as an ideal candidate material for supercapacitor owning to exceptional thermal stability, high surface area, and excellent conductivity. Graphene-based supercapacitors have been reported with a specific capacitance of 135 F g^{-1} in aqueous KOH [3] and 117 F g^{-1} in aqueous H_2SO_4 electrolyte [4].

However, the application of GNS is hindered because of the limited capacitance (usually ~100–200 F g^{-1} [5]). Previous investigations demonstrated that GNS incorporated with nanostructured pseudocapacitive materials (such as Fe_3O_4 [6], Co_3O_4 [7], MnO_2 [8,9], NiO [10]) showed a high energy density. Among them, MnO_2 is one of the most promising pseudocapacitive materials on account of low-cost and environment-friendly [11,12]. Wang's group [13] deposited MnO_2 nanoparticles on the graphene oxide sheets through a simple soft chemical route. It was found that the electrochemical performance was enhanced by the chemical interaction between graphene oxide and MnO_2. In addition, Yan et al. [14] synthesized a composite of graphene/MnO_2 by microwave irradiation and the specific capacitance was up to 310 F g^{-1}. It is noted that electrochemical properties of the composite strongly depended on the morphology and crystallinity of the MnO_2 [15]. Recently, a new composite of carbon nanotubes (CNTs)/graphene, in which CNTs pillars were sandwiched between the graphene layers, has been prepared for SCs [16]. It showed a maximum specific capacitance of 385 F g^{-1}.

Herein, we design a sandwich nanoarchitecture of MnO_2/GNS hybrid with hierarchical structure by a simple but effective strategy, which was assembled by two-dimension (2D) GNS and one-dimension (1D) free-standing needle-like MnO_2 nanowires arrays. By this means, GNS cannot only improve the electron transport for the capacitance reactions but also act as a flexible substrate, while the MnO_2 nanowires arrays can serve as high-capacity hosts and facilitate the penetration of electrolyte. This synthesis method will put forward a new route to produce MnO_2/GNS composite with high performance in large scale at low cost.

2. Experimental

All the chemicals were of analytical grade. Graphite oxide (GO) was synthesized from natural graphite (30 μm) by a modified Hummers method [17]. GNS was prepared from the

*Corresponding author. Tel.: +86 23 65127940; fax: +86 23 65127306.
E-mail address: lixinlu@cqu.edu.cn (X. Li).

0272-8842/$ - see front matter © 2013 Elsevier Ltd and Techna Group S.r.l. All rights reserved.
http://dx.doi.org/10.1016/j.ceramint.2013.06.044

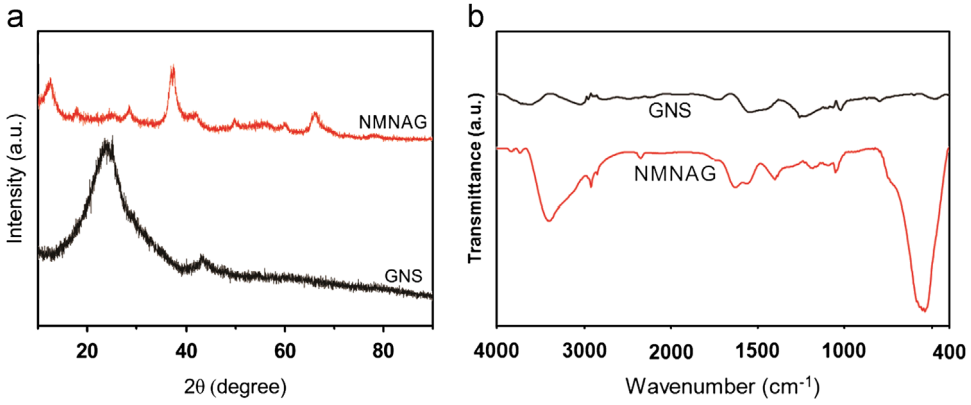

Fig. 1. (a) XRD patterns of GNS and NMNAG and (b) FTIR spectra of GNS and NMNAG.

exfoliated GO by microwave irradiation as described elsewhere [18].

The nanocomposite were synthesized through a simple but effective method. 50 mg of GNS was dispersed in deionized water (100 mL) under ultrasonication for 30 min. Then, potassium permanganate (1 g) was added and the mixture was stirred at room temperature (24 °C) for 6 h. Afterwards, 2 ml concentrated H_2SO_4 was added to the mixture drop by drop. The mixture was heated in a water bath at 80 °C for 1 h. Finally, the product was collected and washed repeatedly with distilled water, then dried at 80 °C for 24 h. The redox reaction can be described in the following:

$$4MnO_4^- + 3C + H_2O = 4MnO_2 + CO_3^{2-} + 2HCO_3^- \quad (1)$$

The crystallographic structure of the materials were analyzed by X-ray diffraction system (XRD, DMAX-2500PC) equipped with Cu Kα radiation (λ=0.15406 nm). Fourier transform infrared spectroscopy (FTIR) spectra were recorded on a GX spectrometer. The morphology was observed by transmission electron microscopy (TEM, LIBRA 200FE) and field-emission scanning electron microscopy (FESEM, ZEISS nova 400), respectively. Brunauer–Emmett–Teller (BET) specific surface area and pore size distribution were measured by nitrogen adsorption/de-adsorption using an automatic adsorption system (ASAP 2020M). Thermogravimetric analysis (TGA) data were collected on a thermal analysis instrument (NETZSCH STA 449C) with a heating rate of 10 °C min^{-1} in an air flow of 50 mL min^{-1}.

The working electrode was prepared by loading the mixture of 70 wt% active materials, 20 wt% carbon black and 10 wt% polyvinylidone difluoride on a nickel foam (1 cm × 1 cm). The mass of MnO_2/GNS on the working electrode was 5.6 mg. All electrochemical measurements were done in a conventional three-electrode configuration. The three-electrode configuration consisted of Pt as the counter electrode, Ag/AgCl as the reference electrode and the above working electrode. The measurements were conducted in a 1 M Na_2SO_4 aqueous electrolyte (pH=9) at room temperature. Cyclic voltammograms (CV) were measured by Solartron (1287+1260 8 w). The galvanostatic charge/discharge and CV were performed within the voltage range from −0.1 to 0.9 V. For the cyclic voltammetric measurements, the sweep rate ranged from 10, 25, 50, 100, and 250 mV s^{-1} and galvanostatic charge/discharge curves were measured at different current densities of 0.5, 1, 2, 5, 10, 20 and 60 A g^{-1}.

3. Results and discussion

Fig. 1(a) presents the XRD patterns of GNS and NMNAG, respectively. Typical peaks of GNS at 2θ=25.9° and 44.2° are observed, corresponding to the diffraction of (0 0 2) and (1 0 0), respectively. As for NMNAG, all diffraction peaks can be indexed to the α-MnO_2 phase (JCPDS no. 44-0141) and no peaks are observed corresponding to other phase of manganese oxides. The FT-IR spectra of GNS and NMNAG are presented in Fig. 1(b). The FTIR spectrum of GNS indicated that the microwave-assisted reduction of GO was relatively completed with few oxygen-containing groups [19]. In the curve of NMNAG, the broad band at 3421 cm^{-1} can be attributed to the O–H stretching vibration of the surface water while the bands centered at 1630, 1399, and 1048 cm^{-1} are associated with the O–H bending vibrations combined with Mn atoms, indicating the presence of bonded water. Furthermore, the presence of the bands at 540 cm^{-1}, which are assigned to the Mn–O vibrations in [MnO_6] octahedral [20], confirming the formation of α-MnO_2 phase.

The morphologies of GNS and NMNAG are shown in Fig. 2. In Fig. 2(a), GNS exhibited a curled and entangled structure. The SEM image (Fig. 2(b)) clearly shows that the free-standing MnO_2 nanowires were grown on the surface of GNS. Notably, the GNS could be viewed as "the substrate" while MnO_2 nanowires could be regarded as the vertical "needles" on the surface. The TEM image (Fig. 2(c)) shows that the needle-like MnO_2 nanowires were oriented on the surface of the GNS, resulting in a sandwich nanoarchitecture. The average diameter of MnO_2 nanowires is ~20 nm and the length is ~200 nm. Fig. 2(d) shows a high-resolution TEM image of the MnO_2 nanowires. The lattice fringes give an interplanar spacing of 0.48 nm, corresponding to the (200) lattice plane of α-MnO_2 crystal, which is in good agreement with the XRD patterns.

The electrochemical performance of the nanocomposite is shown in Fig. 3. Fig. 3(a) presents CV curves of the NMNAG

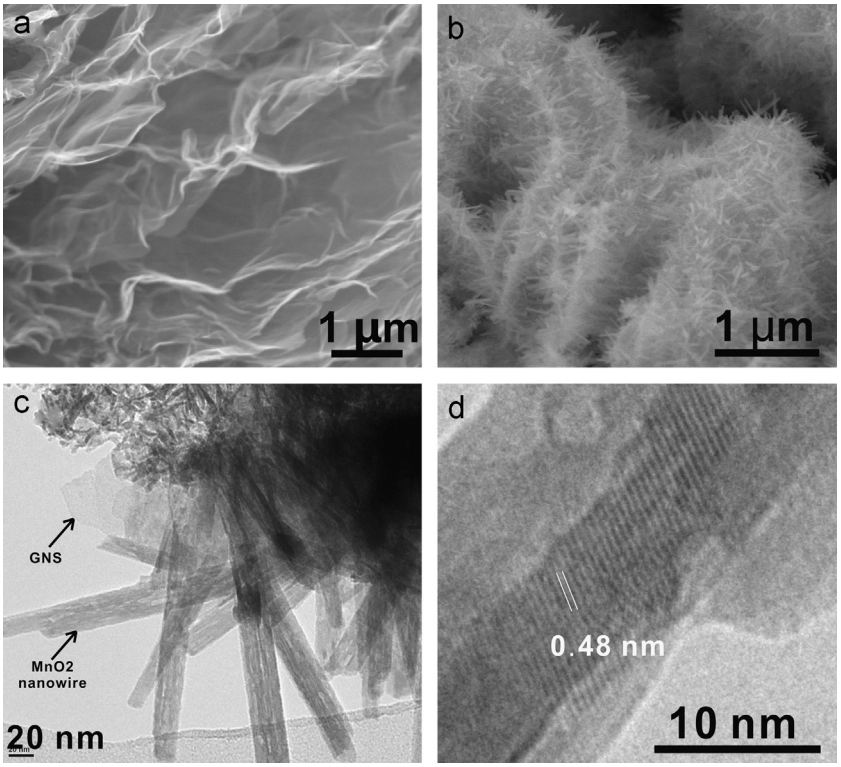

Fig. 2. SEM images of (a) GNS and (b) NMNAG, and (c) TEM images of NMNAG, (d) HRTEM image of the MnO_2 nanowire.

electrode at the scan rates of 10–250 mV s^{-1}. The rectangular and symmetric CV curves reveal the ideal pseudocapacitive nature over the fast charge–discharge process. Moreover, with the the increase of scan rate, all the CV curves do not obviously change and stay nearly rectangular, indicating the stable rate capability. This should be attributed to rapid transport of the electrolyte to the active surface of the hybrid. In comparison, the CV curves of the pristine GNS at 10 mV s^{-1} are also shown in Fig. 3(b). It is obvious that the GNS exhibits a lower specific capacitance as the CV integrated area is much smaller.

Fig. 3(c) illustrates the charge–discharge curves of the NMNAG at different current density. The specific capacitance is calculated according to the discharge curves. At a low current density of 0.5 A g^{-1}, the specific capacitance is up to 276 F g^{-1}, which is remarkably higher than the pristine GNS (81 F g^{-1}). The results are in good accordance with the CV evaluation. Fig. 3(d) shows the specific capacitance of GNS and NMNAG at different current densities. It is noted that the NMNAG electrode exhibits not only a higher specific capacitance, but also a better stability at high current density compared to the bare GNS. As presented in Fig. 3(d), a capacitance of 173 F g^{-1} (~62.7% retention) was retained at the high current density of 60 A g^{-1}. To the best of our knowledge, this capability is superior to or comparable with the previous literatures relative to graphene/MnO_2 composites [8,9,12–14]. The mass loading of MnO_2 in the NMNAG was 98.5% by weight according to the TGA curve, indicating that the MnO_2 almost contributes to the whole capacitance of the NMNAG.

Fig. 4(a) displays the capacitance versus cycle number for NMNAG at 5 A g^{-1}. A slight increase of the initial capacitance can be clearly observed after 1200 cycles due to the activation effect, demonstrating the excellent electrochemical stability. This result has also been confirmed by comparing the charge–discharge curves (inset of Fig. 4a) of 1st cycle and 1200th cycle. Fig. 4(b) shows the Ragone plot of the prepared electrodes. The energy density and power density (based on active materials on both the electrodes) are derived from the charge–discharge curves at different current densities. The energy density reaches 38.3 Wh kg^{-1} at 250 W kg^{-1} power density and still remains 24 Wh kg^{-1} at 21.6 kW kg^{-1} power density. This performance is significantly better than those of recently reported MnO_2–graphene [21,22], NiO–graphene [23], and RuO_2–graphene [24] composites.

The high rate capability and excellent cycling stability of the needle-like MnO_2 nanowires arrays/graphene nanocomposite would provide a big forward for high-performance supercapacitors. In the 3D nanoarchitecture, the graphene conductive network improves the electron conductivity of MnO_2, facilitating the rapid charge transport. The needle-like nanowires arrays can enlarge the interface area between MnO_2 and electrolyte, thus improving the pseudocapacitance occurring at the interface. And the ordered space between the free-standing MnO_2 nanowires can act as a buffer to alleviate the volume expansion of the MnO_2 during the charge/discharge process.

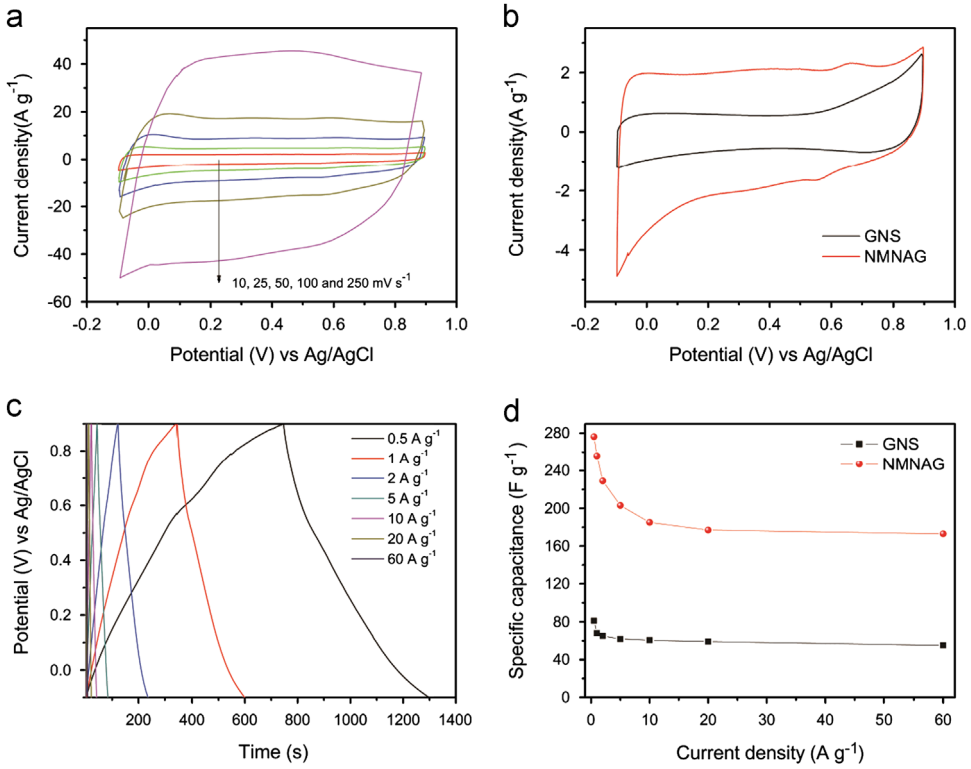

Fig. 3. (a) Cyclic voltammograms obtained from NMNAG electrode at different sweep rates. (b) CV curves of GNS and NMNAG at scan rate of 10 mV s^{-1}. (c) charge–discharge curves of NMNAG at different density. (d) The specific capacitance as a function of different current density of the NMNAG and the pristine GNS. (For interpretation of the references to color in this figure legend, the reader is referred to the web version of this article.)

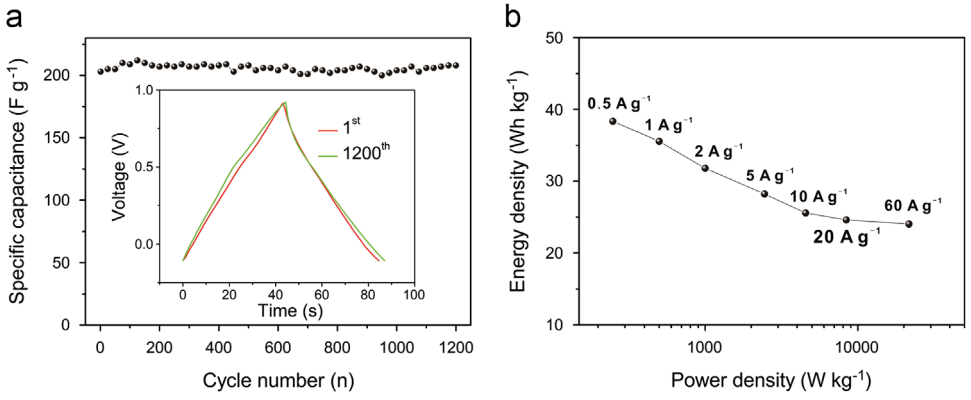

Fig. 4. (a) Specific capacitance as a function of cycle number at 5 A g^{-1} of the NMNAG electrodes. Insets show 1st cycle and 1200th cycle of the NMNAG electrodes. (b) Ragone plot (power density vs. energy density) of the NMNAG electrodes. The energy densities and power densities were derived from the charge–discharge curves at different current densities.

4. Conclusions

In summary, we have prepared the nanoarchitecture of MnO_2/GNS composite with hierarchical structure by a simple but effective method, in which free-standing needle-like MnO_2 nanowires arrays were sandwiched between graphene nanosheets. The integration of GNS and the free-standing needle-like MnO_2 nanowires endows the hybrid with good capacitive performance. The intriguing nanoarchitecture combining the free-standing MnO_2 nanowires arrays with the flexible, large surface area and highly conductive GNS will offer great promise in high-power energy storage device applications.

Acknowledgments

We are grateful for the financial support from Project no. CDJZR12 22 55 01 & of the Fundamental Research Funds for the Central Universities and for the Natural Science Foundation of China (No. 51172293).

References

[1] B.E. Conway, Electrochemical Supercapacitors: Scientific Fundamentals and Technological Applications, Plenum Publishers, New York, 1999.

[2] K.S. Novoselov, A.K. Geim, S.V. Morozov, D. Jiang, Y. Zhang, S.V. Dubonos, I.V. Grigorieva, A.A. Firsov, Electric field effect in atomically thin carbon films, Science 306 (5696) (2004) 666–669.

[3] M.D. Stoller, S. Park, Y. Zhu, J. An, R.S. Ruoff, Graphene-based ultracapacitors, Nano Letters 8 (10) (2008) 3498–3502.

[4] S. Vivekchand, C. Rout, K. Subrahmanyam, A. Govindaraj, C. Rao, Graphene-based electrochemical supercapacitors, Journal of Chemical Sciences 120 (1) (2008) 9–13.

[5] S. Bose, T. Kuila, A.K. Mishra, R. Rajasekar, N.H. Kim, J.H. Lee, Carbon-based nanostructured materials and their composites as supercapacitor electrodes, Journal of Materials Chemistry 22 (3) (2012) 767–784.

[6] Q. Qu, S. Yang, X. Feng, 2D sandwich-like sheets of iron oxide grown on graphene as high energy anode material for supercapacitors, Advanced Materials 23 (46) (2011) 5574–5580.

[7] X.-C. Dong, H. Xu, X.-W. Wang, Y.-X. Huang, M.B. Chan-Park, H. Zhang, L.-H. Wang, W. Huang, P. Chen, 3D graphene–cobalt oxide electrode for high-performance supercapacitor and enzymeless glucose detection, ACS Nano 6 (4) (2012) 3206–3213.

[8] C.-Y. Chen, H.-W. Chang, S.-J. Shih, C.-Y. Tsay, C.-J. Chang, C.-K. Lin, High supercapacitive stability of spray pyrolyzed ZnO-added manganese oxide coatings, Ceramics International 39 (2) (2013) 1885–1892.

[9] D.P. Dubal, C.D. Lokhande, Significant improvement in the electrochemical performances of nano-nest like amorphous MnO_2 electrodes due to Fe doping, Ceramics International 39 (1) (2013) 415–423.

[10] B. Zhao, J. Song, P. Liu, W. Xu, T. Fang, Z. Jiao, H. Zhang, Y. Jiang, Monolayer graphene/NiO nanosheets with two-dimension structure for supercapacitors, Journal of Materials Chemistry 21 (46) (2011) 18792–18798.

[11] W. Wei, X. Cui, W. Chen, D.G. Ivey, Manganese oxide-based materials as electrochemical supercapacitor electrodes, Chemical Society Reviews 40 (3) (2011) 1697–1721.

[12] S.K. Meher, G.R. Rao, Enhanced activity of microwave synthesized hierarchical MnO_2 for high performance supercapacitor applications, Journal of Power Sources 215 (0) (2012) 317–328.

[13] S. Chen, J. Zhu, X. Wu, Q. Han, X. Wang, Graphene Oxide–MnO_2 nanocomposites for supercapacitors, ACS Nano 4 (5) (2010) 2822–2830.

[14] J. Yan, Z. Fan, T. Wei, W. Qian, M. Zhang, F. Wei, Fast and reversible surface redox reaction of graphene–MnO_2 composites as supercapacitor electrodes, Carbon 48 (13) (2010) 3825–3833.

[15] L. Mao, K. Zhang, H.S. On Chan, J. Wu, Nanostructured MnO_2/graphene composites for supercapacitor electrodes: the effect of morphology, crystallinity and composition, Journal of Materials Chemistry 22 (5) (2012) 1845–1851.

[16] Z. Fan, J. Yan, L. Zhi, Q. Zhang, T. Wei, J. Feng, M. Zhang, W. Qian, F. Wei, A Three-Dimensional, Carbon nanotube/graphene sandwich and its application as electrode in supercapacitors, Advanced Materials 22 (33) (2010) 3723–3728.

[17] W.S. Hummers, R.E. Offeman, Preparation of graphitic oxide, Journal of the American Chemical Society 80 (6) (1958) 1339.

[18] L. Xinlu, S. Hongfang, W. Hao, L. Hongyi, Z. Yuxin, H. Jiamu, A comparison of exfoliation methods on microstructure and electrochemical performance of graphene nanosheets for supercapacitors, Journal of New Materials for Electrochemical Systems 15 (2) (2012) 097–101.

[19] Y. Zhu, S. Murali, M.D. Stoller, A. Velamakanni, R.D. Piner, R.S. Ruoff, Microwave assisted exfoliation and reduction of graphite oxide for ultracapacitors, Carbon 48 (7) (2010) 2118–2122.

[20] M.V. Ananth, S. Pethkar, K. Dakshinamurthi, Distortion of MnO_6 octahedra and electrochemical activity of Nstutite-based MnO_2 polymorphs for alkaline electrolytes—an FTIR study, Journal of Power Sources 75 (2) (1998) 278–282.

[21] Z.-S. Wu, W. Ren, D.-W. Wang, F. Li, B. Liu, H.-M. Cheng, High-energy MnO_2 nanowire/graphene and graphene asymmetric electrochemical capacitors, ACS Nano 4 (10) (2010) 5835–5842.

[22] L. Deng, G. Zhu, J. Wang, L. Kang, Z.-H. Liu, Z. Yang, Z. Wang, Graphene–MnO_2 and graphene asymmetrical electrochemical capacitor with a high energy density in aqueous electrolyte, Journal of Power Sources 196 (24) (2011) 10782–10787.

[23] X. Xia, J. Tu, Y. Mai, R. Chen, X. Wang, C. Gu, X. Zhao, Graphene sheet/porous NiO hybrid film for supercapacitor applications, Chemistry–A European Journal 17 (39) (2011) 10898–10905.

[24] Z.-S. Wu, D.-W. Wang, W. Ren, J. Zhao, G. Zhou, F. Li, H.-M. Cheng, Anchoring hydrous RuO_2 on graphene sheets for high-performance electrochemical capacitors, Advanced Functional Materials 20 (20) (2010) 3595–3602.